A Seamless Magnetization State Transition Strategy for Variable Flux Machines Based on Direct Flux Vector Control

A Seamless Magnetization State Transition Strategy for Variable Flux Machines Based on Direct Flux Vector Control

Chen Chen
Dept. of Energy "Galileo Ferraris"
Politecnico di Torino
Torino, Italy
chen_chen@polito.it

Raffaele Garino
Dept. of Energy "Galileo Ferraris"
Politecnico di Torino
Torino, Italy
raffaele.garino@polito.it

Paolo Pescetto
Dept. of Energy "Galileo Ferraris"
Politecnico di Torino
Torino, Italy
paolo.pescetto@polito.it

Simone Ferrari
Dept. of Energy "Galileo Ferraris"
Politecnico di Torino
Torino, Italy
simone.ferrari@polito.it

Gianmario Pellegrino
Dept. of Energy "Galileo Ferraris"
Politecnico di Torino
Torino, Italy
gianmario.pellegrino@polito.it

***Abstract*—This paper proposes a control strategy for regulating the Magnetization State (MS) of Variable Flux Machines (VFMs) under load conditions, avoiding torque perturbations caused by the required high-amplitude magnetization current pulses. The proposed approach is implemented as a modification of a standard Direct Flux Vector Control (DFVC) scheme, adjusting the flux magnitude control law. MS manipulation is achieved through calibrated flux pulses derived from precomputed magnetization maps. The proposed control scheme is validated through simulation based on a prototype surface-PM Variable Flux Machine.**

***Index Terms*—Variable Flux Machines, Memory Motors, DFVC, Flux Maps, Irreversible Demagnetization, Torque continuity.**

I. Introduction

Variable Flux Machines (VFMs) are a category of Permanent Magnet Synchronous Machines (PMSMs) employing rare-earth-free, low-coercivity magnets whose Magnetization State (MS) can be dynamically regulated through dedicated current pulses during operation [1]–[4]. This requires tailored methods for torque control and flux estimation, [5], [6] compared to standard PMSMs [7], [8], but allows to extend the maximum torque Vs speed envelop while optimizing the motor efficiency over a drive cycle [9]–[11], as illustrated in Fig. 1.

When operated under load, the current pulses injected for MS manipulation may seriously perturb torque, with user discomfort and risk of control loss. In traction applications, for example, such disturbances would be perceived by passengers as undesirable speed bumps. Mitigating these torque perturbations is not merely a matter of performance optimization, but a prerequisite for the effective and widespread adoption of this technology. Several studies have addressed torque perturbations during MS transitions. In [12], three different strategies are investigated. The first approach injects only a d-axis current component while keeping i_q=0. This is only applicable under no-load conditions, as torque disturbances inevitably arise under load. The second method determines, for a given magnetizing current required to reach the target MS, the corresponding i_q trajectory through precomputed lookup tables, achieving disturbance-free torque production. However, this approach requires extensive experimental characterization or computationally intensive FEA campaigns to derive the current trajectories for every combination of load condition and magnetization state at different temperatures. To overcome these limitations, the same Authors propose an observer-based current decoupling method, where decoupling current components are superimposed on the MTPA current references. While effective in principle, this solution relies on a complex observer architecture composed of a stator current observer cascaded with a Gopinath style stator flux linkage observer based on voltage disturbance estimation, resulting in considerable implementation complexity. In [13], two modified i_q reference generation methods are proposed for MS regulations. The first one is based on the enforcement of

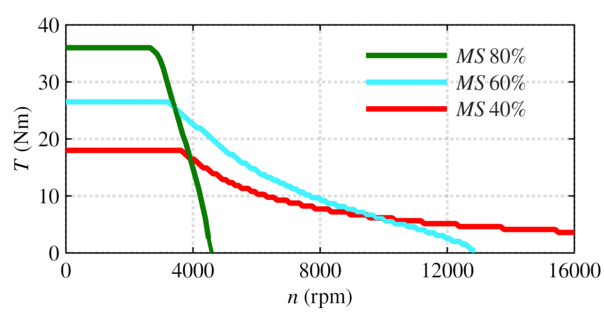

Fig. 1: Torque-speed profile at 25Apk, 600Vdc.

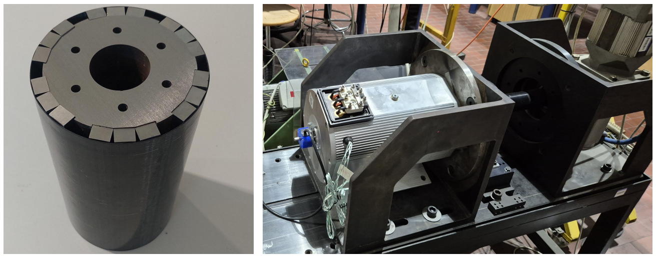

Fig. 2: VFM prototype.

TABLE I: Ratings of the motor under test

Maximum torque	35 Nm
Max operating current	25 A-pk
Base speed at MS80%	2600 rpm
Max remag current	70 A-pk
Max speed	12000 rpm
DC-link voltage	600 V
Pole Pairs	3

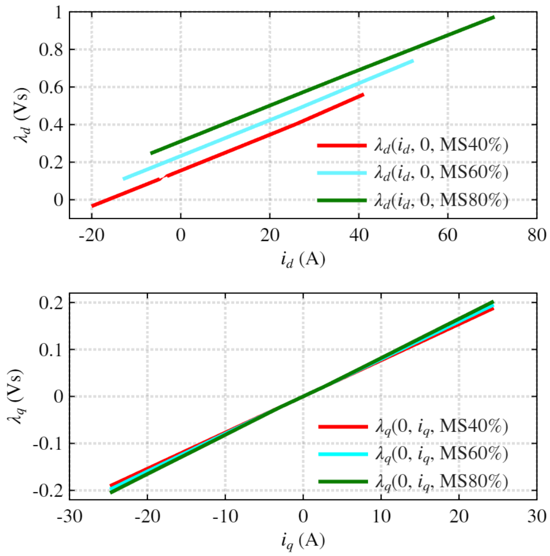

Fig. 3: FEA calculated saturation curves for different MSs of MUT: $\lambda_d\left(i_d, 0, MS\right)$ and $\lambda_q\left(0, i_q, MS\right)$.

the inverter voltage limit constrain while the second is based on the torque equation neglecting the change in the speed, yet torque peaks are not effectively suppressed. In [14] a sliding-mode speed loop combined with MPC current loop is proposed, increasing control complexity while providing limited torque pulse mitigation. Furthermore, this method is inherently designed for operating within a closed-loop speed control scheme, and it's not compatible with torque controlled applications such as automotive traction systems. Finally, [15] proposes a dedicated compensation scheme for dual three-phase VFMs, demonstrating effective torque disturbance suppression. However, its applicability is inherently limited to dual three-phase machine topologies and cannot be directly extended to conventional three-phase VFMs.

In this scenario, this article proposes a modified Direct Flux Vector Control (DFVC) strategy that inherently combines torque control and magnetization state regulation within a single control framework. The proposed method minimizes torque disturbances during both magnetization and demagnetization processes while extending the same control architecture to steady state MS operation and flux-weakening operation by simply adapting the stator flux reference.

II. Motor Under Test

The Motor Under Test (MUT) is a surface-mounted permanent magnet synchronous machine (SPM-PMSM) employing AlNiCo 5 permanent magnets and a carbon-fiber retaining sleeve to ensure the mechanical integrity of the rotor at high rotational speeds. The machine has been specifically designed as a scaled-down prototype of a VFM intended for hybrid and full-electric traction applications. The manufactured prototype is shown in Fig. 2, while the corresponding torque-speed envelopes at different magnetization states (MSs) are reported in Fig. 1. The main machine ratings are summarized in Tab. I, and the FEA calculated saturation characteristics are presented in Fig. 3.

The adoption of a SPM rotor topology was primarily motivated by its suitability for controlled magnetization state regulation under load. Unlike interior permanent magnet (IPM) or reluctance-assisted topologies, the SPM configuration enables continuous torque production over the entire magnetization range without crossing a zero-torque locus during either magnetization or demagnetization transients. This characteristic is a prerequisite for torque-preserving magnetization state control, as it allows the machine to undergo magnetization state transitions without losing torque capability, thus enabling controlled suppression of torque disturbances. A detailed discussion of this aspect can be found in [16].

III. Variable Flux Machine Model

The motor model is formulated in the rotor reference frame dq, with complex quantities indicated in **bold**. The complex magnetization state is defined as:

$$\boldsymbol{MS} = \frac{\lambda_m}{\lambda_{m,max}} \cdot e^{j\phi_{MS}} \;=\; MS \cdot e^{j\phi_{MS}} \tag{1}$$

where λ_m is the PM flux linkage magnitude and $\lambda_{m,\max}$ is its value at full magnetization. The stator voltage equation and magnetic model are expressed as:

$$\boldsymbol{v}_{dq} = R_s \boldsymbol{i}_{dq} + \frac{d\boldsymbol{\lambda}_{dq}}{dt} + \omega \boldsymbol{J} \boldsymbol{\lambda}_{dq} \tag{2}$$

$$\begin{cases} \lambda_d = \lambda_d(\boldsymbol{i}_{dq}, \boldsymbol{MS}) \\ \lambda_q = \lambda_q(\boldsymbol{i}_{dq}, MS) \end{cases} \tag{3}$$

where R_s is the stator resistance, $\boldsymbol{v}_{dq}$, $\boldsymbol{i}_{dq}$, and $\boldsymbol{\lambda}_{dq}$ are the stator voltage, current, and flux linkage vectors, ω is the angular frequency, and $\boldsymbol{J}$ is the imaginary unit matrix.

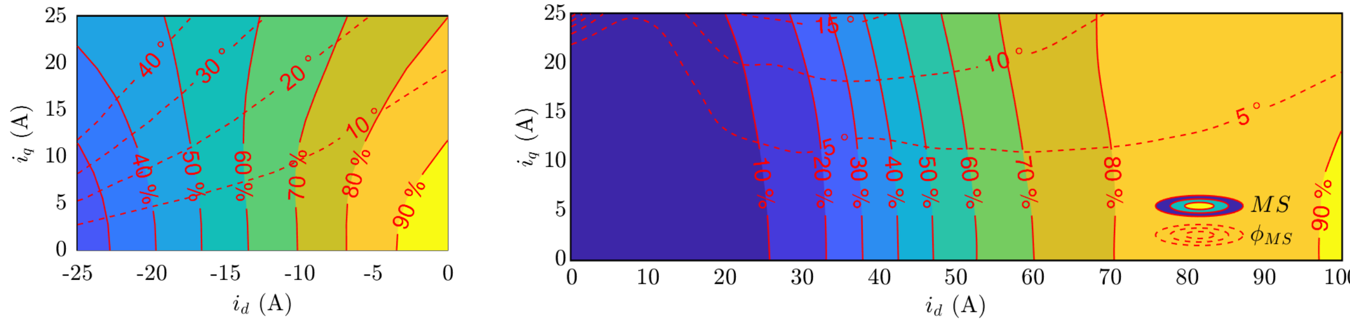

Fig. 4: Demag (left) and Remag (right) maps defined in the current dq plane.

A. Magnetization and Demagnetization Maps

The two complex Demagnetization and Remagnetization Look-up-Tables (LUTs) shown in Fig. 4 are computed via FEA and represent the $\boldsymbol{MS}$, in magnitude and phase, function of i_d and i_q. Starting with the PM fully magnetized (MS=100% and ϕ_{MS}=0), the **Demag map** depicts the $\boldsymbol{MS}$ variation when the VFM is subject to a demagnetizing current in the 2nd quadrant. Similarly, the **Remag map** represents the $\boldsymbol{MS}$ function of a magnetizing current vector imposed in the 1st quadrant starting from MS = 0%.

These LUTs can be obtained either through FEA or experimentally. The machine is driven at constant speed while a magnetizing or demagnetizing current vector is applied at a selected operating point in the current plane. The current is then brought back to zero, and the no-load back-EMF is measured. From this back-EMF, the PM flux linkage is calculated, and so the corresponding magnetization state. A detailed description of the characterization procedure is provided in [17], [18].

B. Simulation model

The VFM simulation model, implemented in a MATLAB-Simulink environment, is based on a circuital Controlled Current Generator (CCG) approach [19], [20], extended to account for $\boldsymbol{MS}$ variations through two additional blocks: the modified inverse flux maps, highlighted in green, and the Demagnetization/Remagnetization tables, highlighted in red, as shown in Fig. 5. The complete formulation and implementation details of the model have been extensively described in the authors' previous publications [17], [21], and not repeated here, as they fall outside the scope of this paper.

IV. Proposed Control Strategy

A. Direct Flux Vector Control Background

The Direct Flux Vector Control (DFVC) strategy is developed in the stator flux reference frame, $d_s q_s$, shown in Fig. 6, with d_s aligned to the stator flux linkage vector [22]. In such coordinates, the voltage and torque equations are (4), (5), where λ is the magnitude of $\boldsymbol{\lambda}_{dq}$ and δ is its phase angle with respect to the d-axis, also referred as load angle.

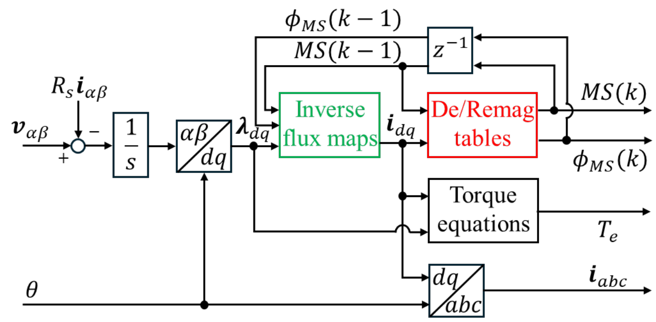

Fig. 5: Electromagnetic model of VFMs able to capture asymmetrical magnetization of PM.

$$\begin{cases} v_{ds} = R_s i_{ds} + \dfrac{d\lambda}{dt} \\ v_{qs} = R_s i_{qs} + \lambda\left(\omega + \dfrac{d\delta}{dt}\right) \end{cases} \tag{4}$$

$$T = \frac{3}{2} p \lambda i_{qs} \tag{5}$$

The flux magnitude λ and its quadrature current component i_{qs} are closed-loop controlled following the torque setpoint as shown in Fig. 7. During steady MS operation the DFVC sets the reference flux magnitude λ^* based on the MTPA (blue dashed box of Fig. 7), as a function of the estimated $\widehat{MS}$ (6). The flux magnitude is then saturated by the Flux Weakening (FW) block according to the motor speed and DC-link voltage. The quadrature current reference i_{qs}^* is computed from torque

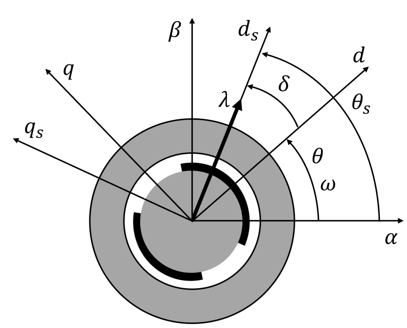

Fig. 6: Stator flux reference frame

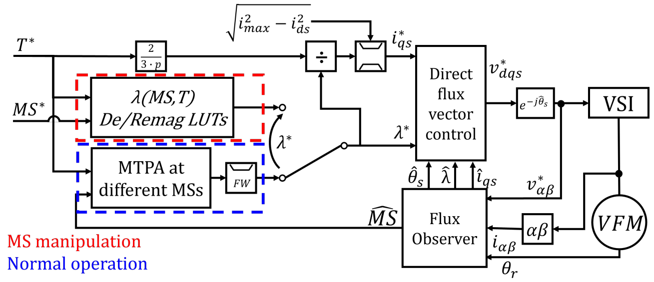

Fig. 7: Proposed DFVC control scheme

and flux reference based on (7), and it is saturated to meet the inverter current limit i_{max}.

$$\lambda^* = \lambda^* \left(T^*, \widehat{MS} \right) \tag{6}$$

$$i_{qs}^* = \frac{T^*}{\frac{3}{2} p \lambda^*} \tag{7}$$

B. DFVC for MS Manipulation

When a change in $\boldsymbol{MS}$ is commanded, the control switches to MS manipulation (red dashed box of Fig. 7). The Demag/Remag maps replace the MTPA law and set the appropriate reference flux linkage.

$$\lambda^* = \begin{cases} \lambda_{\text{remag}} \left(MS_{\text{remag}}^*, T^* \right) \\ \lambda_{\text{demag}} \left(MS_{\text{demag}}^*, T^* \right) \end{cases} \tag{8}$$

The rest of torque control is unchanged: upon λ^* variation, i_{qs}^* is is updated based on (7), guaranteeing torque continuity during MS transitions. Otherwise said, the flux control is in charge of MS manipulation, while the i_{qs} control permits to maintain accurate torque control. Once the target MS^* is reached, the controller returns to normal operating mode and λ^* is again based on the MTPA law.

C. Manipulation of Demag and Remag Maps

The key for an accurate MS manupulation is the correct determination of λ^* during MS transients. To this aim, the Demag and Remag maps of Fig. 4 are manipulated to express the flux linkage magnitude as a function of MS and torque:

$$MS\left(i_d, i_q\right) \;\rightarrow\; \lambda\left(MS, T\right) \tag{9}$$

Such tables are used for generating the flux reference during the MS variation process. The LUTs manipulation requires computing the torque and flux magnitude per each point of the Demag and Remag maps in Fig. 4.

$$T = \frac{3}{2} p [\lambda_d(i_d, i_q, MS) \cdot i_q - \lambda_q(i_d, i_q, MS) \cdot i_d] \tag{10}$$

$$\lambda = \sqrt{\lambda_d^2 + \lambda_q^2} \tag{11}$$

Therefore, the demagnetization and remagnetization characteristics can be expressed in the torque and flux domain, defining the LUTs $\lambda(MS_{demag}^*, T^*)$ and $\lambda(MS_{remag}^*, T^*)$. These are reported in fig. 8. In this way, the control system can directly generate the flux reference needed for the desired MS target at a given torque level, without explicitly estimating the full dq current trajectory.

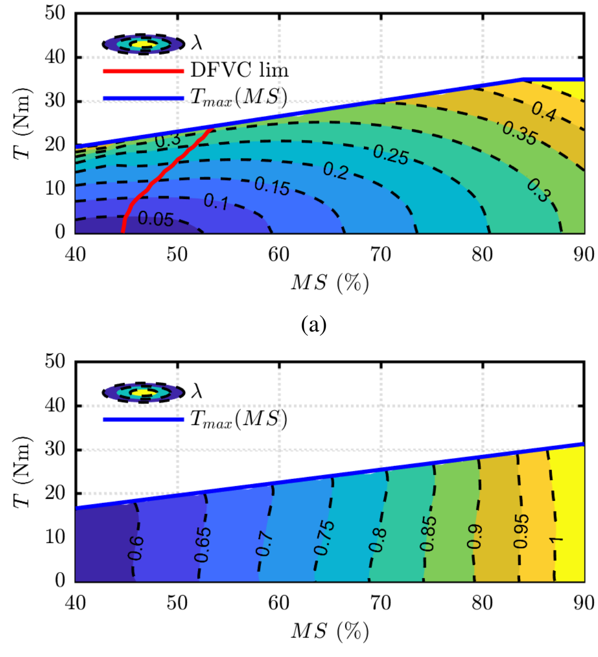

(b)

Fig. 8: Inverse Demag (a) and inverse Remag (b) maps defined in the torque and MS domain.

D. DFVC Demagnetization Limit

The feasible remagnetization region under DFVC is limited. The red line in the Demag map, Fig. 8.a, indicates the lower boundary of the DFVC-based demagnetization process for this machine. The flux amplitude contours have a circular shape, and gradually become horizontal as MS decreases and T increases. This behavior occurs when the operating point approaches the MTPV region. In this condition, the sign of the feedback signal reverses, causing the control input to diverge and the control to become unstable.

This limitation does not affect the remagnetization process, as can be noticed in Fig. 8.b, the flux contours are vertical or pseudo-vertical, meaning that the sign of the feedback signal does not change. Therefore, stable control is maintained during remagnetization.

E. Flux observer

The flux observer is a key building block of DFVC-based motor control, since accurate knowledge of the flux vector is required both for torque control and online estimation of the magnetization state. The proposed control strategy for MS manipulation with reduced torque disturbance can be associated with any type of flux observer suitable for VFMs [23], [24], e.g., including the $\boldsymbol{MS}$ variability in the

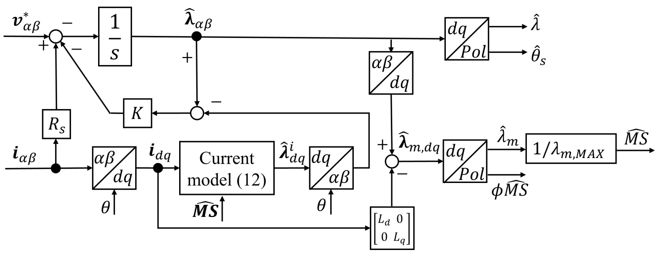

Fig. 9: Block diagram of the flux observer.

flux estimation. The flux observer in Fig. 9 is proposed here, with embedded $\boldsymbol{MS}$ estimation.

The observer is based on a classical hybrid flux observer structure [25]–[27], combining a voltage-model estimator with a current-model correction loop. The voltage model reconstructs the stator flux vector through back-EMF integration, whereas the current model computes the expected flux vector according to (12).

$$\hat{\boldsymbol{\lambda}}^i_{dq} = \widehat{MS} \cdot \lambda_{m,\max} \cdot e^{j\phi\widehat{MS}} + \begin{bmatrix} L_d & 0 \\ 0 & L_q \end{bmatrix} \cdot \boldsymbol{i}_{dq} \tag{12}$$

The proposed one is further extended by embedding an online estimation of the magnetization state. After reconstructing the stator flux vector, the armature contribution is removed based in the machine inductances, obtaining an estimate of the PM flux vector:

$$\begin{aligned} \hat{\lambda}_{m,d} &= \hat{\lambda}_d - L_d \cdot i_d \\ \hat{\lambda}_{m,q} &= \hat{\lambda}_q - L_q \cdot i_q \end{aligned} \tag{13}$$

The estimated PM flux vector is then used to determine the $\boldsymbol{MS}$ magnitude and phase according to (1). Then, the complex estimated magnetization state is finally fed back to the current model. Finally, the estimated flux angle $\widehat{\theta}_s$ is calculated as:

$$\widehat{\theta}_s = \tan^{-1} \frac{\hat{\lambda}_\beta}{\hat{\lambda}_\alpha} \tag{14}$$

V. Simulation Results

The control strategy is validated in MATLAB-Simulink environment, in which the digital controller, inverter and motor are modeled. The simulation results are represented in Fig. 10. The machine initially operates at $MS = 80\%$, accelerates to 1000 rpm, and is loaded with a constant reference torque of 12 Nm throughout the entire test. A demagnetization command to $MS^* = 50\%$ is then applied, followed by a remagnetization command back to $MS^* = 80\%$. As can be observed, the controlled variables closely track their references throughout the entire test. In particular, MS accurately follows its target MS^*, while the residual torque perturbation only presents short-duration spikes within ± 2 Nm during both demagnetization and remagnetization transients.

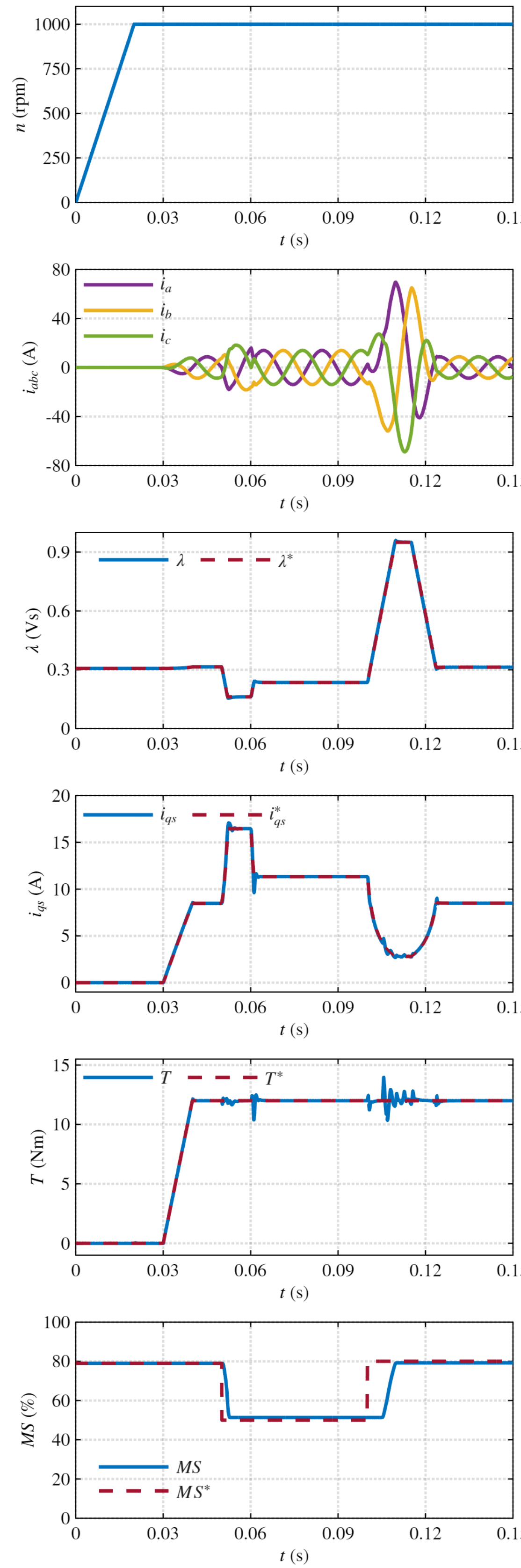

Fig. 10: Simulation test results: mechanical speed, phase currents, flux magnitude, q_s-axis current, torque, and MS.

The flux behavior shown in Fig. 10 further clarifies the control action. The machine starts with a constant reference flux amplitude of 0.30 Vs, corresponding to the MTPA at T^*=12 Nm, MS=80%. During the demagnetization transient, the flux reference is reduced to 0.16 Vs to drive the machine toward the target $MS = 50\%$. Once the demagnetization process is completed, the reference flux returns to 0.23 Vs, corresponding to the MTPA point at MS=50%. Subsequently, during remagnetization, a flux pulse of 0.95 Vs is applied, after which the reference settles again to 0.31 Vs when the machine returns to $MS = 80\%$. As can be noted, i_{qs}^* is correspondingly updated based on (7), thus maintaining smooth torque control during the whole process, without requiring explicit prediction of the full current trajectory in the dq plane.

A. Deep demagnetization test

An example of deep demagnetization test is shown in Fig. 11. This is performed at the same speed of 1000 rpm, but with torque reference of $T^* = 16$ Nm and target magnetization state of $MS^* = 40\%$. Unlike the previous case, the control becomes unstable and fails to converge to the desired MS^*. This behavior is expected since the target operating point lies beyond the red limit boundary shown in Fig. 8.a, where no feasible steady-state solution exist for the DFVC strategy. As the controller attempts to track an unattainable flux reference while simultaneously regulating the torque, the current deviates from the desired trajectory, eventually leading to instability.

VI. Conclusions and Future Works

This paper presents a Direct Flux Vector Control strategy specifically developed for Variable Flux Machines, enabling both magnetization state regulation and torque control within a unified control framework. By directly controlling the stator flux magnitude and quadrature current, the proposed approach achieves smooth magnetization and demagnetization transients while preserving the commanded torque, thereby minimizing torque disturbances typically associated with magnetization state variations. Furthermore, the same control structure naturally extends from the constant-torque region to flux-weakening operation by simply adapting the stator flux reference, without requiring any modification of the control architecture or additional LUTs. Compared to existing techniques, the proposal does not require to pre-calculate specific current trajectories to maintain seamless torque control during MS transients, thus considerably simplifying the control calibration. Simulation results demonstrated the effectiveness of the proposed strategy under both magnetization and moderate demagnetization operating conditions. However, the analysis also highlighted an intrinsic limitation of the DFVC approach during deep demagnetization. When the requested combination of torque and magnetization state lies outside the feasible operating region, no steady-state solution exists and the controller is unable to converge to the desired operating point. Consequently, the proposed strategy is inherently limited to the feasible demagnetization region of the machine.

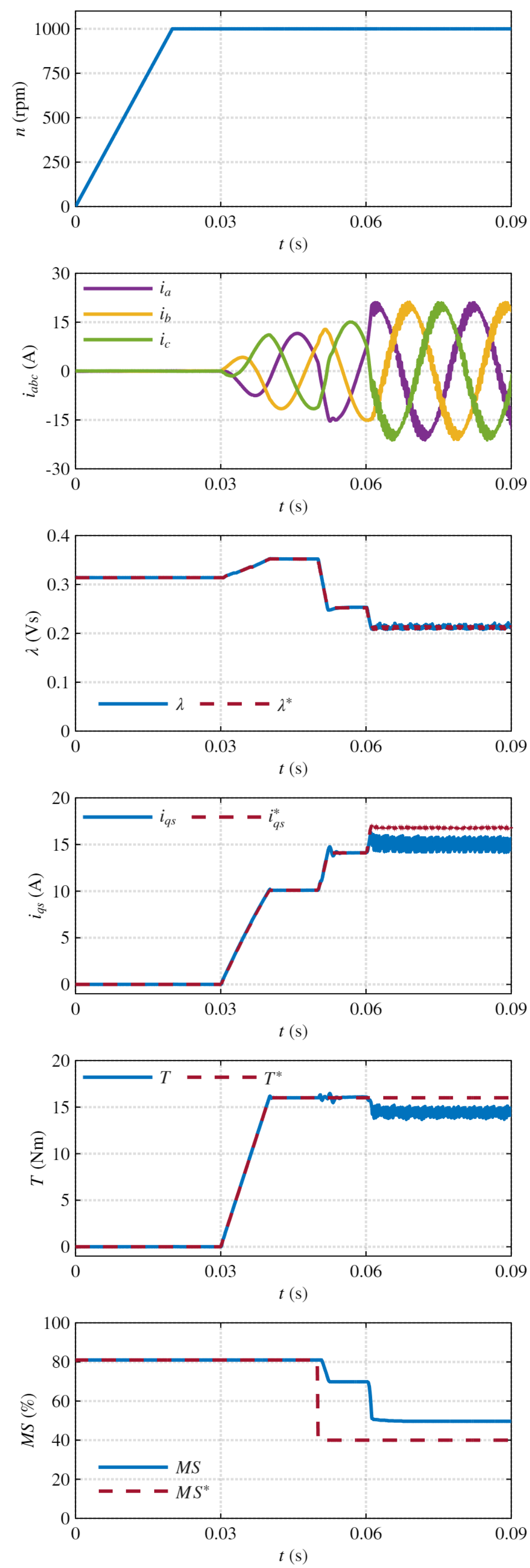

Fig. 11: Deep demagnetization test simulation results: mechanical speed, phase currents, flux magnitude, q_s-axis current, torque, and MS.

Future work will focus on overcoming this limitation. In addition, the proposed control strategy is currently being implemented and experimentally validated on the VFM prototype, reported in Fig. 2, to assess its performance under realistic operating conditions.

ACKNOWLEDGMENT

The research has been conducted with the support of Power Electronics Innovation Center (PEIC) of Politecnico di Torino.

The research was supported by the project REVEAL, supported by *Fondazione Compagnia di San Paolo*.

REFERENCES

[1] V. Ostovic, "Memory motors," *IEEE Industry Applications Magazine*, vol. 9, no. 1, 2003.

[2] H. Yang, Z. Q. Zhu, H. Lin, S. Fang, and Y. Huang, "Comparative study of novel variable-flux memory machines having stator permanent magnet topologies," *IEEE Transactions on Magnetics*, vol. 51, no. 11, pp. 1–4, 2015.

[3] A. M. Aljehaimi and P. Pillay, "Novel flux linkage estimation algorithm for a variable flux pmsm," *IEEE Transactions on Industry Applications*, vol. 54, no. 3, pp. 2319–2335, 2018.

[4] G. Qiao, M. Wang, F. Liu, Y. Liu, and P. Zheng, "Analysis of novel hybrid-pm variable-flux pmsms with series–parallel magnetic circuits," *IEEE Transactions on Magnetics*, vol. 57, no. 2, pp. 1–6, 2021.

[5] D. F. Laborda, D. Díaz Reigosa, D. Fernández, K. Sasaki, T. Kato, and F. Briz, "Magnet temperature estimation in variable leakage flux permanent magnet synchronous machines using the magnet flux linkage," in *2020 IEEE Energy Conversion Congress and Exposition (ECCE)*, 2020, pp. 6111–6117.

[6] D. F. Laborda, D. D. Reigosa, D. Fernández, K. Sasaki, T. Kato, and F. Briz, "Enhanced torque estimation in variable leakage flux pmsm combining high and low frequency signal injection," *IEEE Transactions on Industry Applications*, vol. 59, no. 1, pp. 801–813, 2023.

[7] A. Bojoi, P. Pescetto, S. Ferrari, and G. Pellegrino, "Torque ripple map of synchronous machines via manipulation of experimental $dq\theta$ flux maps: Implementation and validation," *IEEE Transactions on Industry Applications*, pp. 1–10, 2026.

[8] A. J. P. Ortega, S. Das, R. Islam, and M. B. Kouhshahi, "High-fidelity analysis with multiphysics simulation for performance evaluation of electric motors used in traction applications," *IEEE Transactions on Industry Applications*, vol. 59, no. 2, pp. 1273–1282, 2023.

[9] T. Fukushige, N. Limsuwan, T. Kato, K. Akatsu, and R. D. Lorenz, "Efficiency contours and loss minimization over a driving cycle of a variable flux-intensifying machine," *IEEE Transactions on Industry Applications*, vol. 51, no. 4, pp. 2984–2989, 2015.

[10] A. Athavale, T. Fukushige, T. Kato, C.-Y. Yu, and R. D. Lorenz, "Variable leakage flux ipmsms for reduced losses over a driving cycle while maintaining suitable attributes for high-frequency injection-based rotor position self-sensing," *IEEE Transactions on Industry Applications*, vol. 52, no. 1, pp. 234–241, 2016.

[11] X. Yu, X. Zhu, L. Quan, Z. Xiang, and D. Fan, "Investigation and regulation of high-efficiency region boundary of variable magnetic flux permanent magnet motor," *Chinese Journal of Electrical Engineering*, vol. 10, no. 3, pp. 135–146, 2024.

[12] C.-Y. Yu, T. Fukushige, N. Limsuwan, T. Kato, D. D. Reigosa, and R. D. Lorenz, "Variable-flux machine torque estimation and pulsating torque mitigation during magnetization state manipulation," *IEEE Transactions on Industry Applications*, vol. 50, no. 5, pp. 3414–3422, 2014.

[13] B. Basnet and P. Pillay, "Torque pulsation reduction during magnetization in variable flux machines," *IEEE Journal of Emerging and Selected Topics in Power Electronics*, vol. 10, no. 2, pp. 1703–1711, 2022.

[14] H. Huang, H. Yang, X. Liu, and Y. Zhong, "A novel model predictive control for torque pulsations suppression of variable flux memory machine during magnetization state manipulations," in *2023 26th International Conference on Electrical Machines and Systems (ICEMS)*, 2023, pp. 3931–3936.

[15] X. Liu, H. Hua, W. He, and W. Hua, "Comprehensive investigation of pulsating torque suppressions of variable flux memory machines during magnetization state regulations," *IEEE Transactions on Industrial Electronics*, vol. 72, no. 12, pp. 12 611–12 620, 2025.

[16] C. Chen, R. Garino, P. Pescetto, S. Ferrari, and G. Pellegrino, "Comparative analysis of rotor topologies in variable flux machines with low coercivity magnets," in *2026 IEEE International Conference on Electrical Machines (ICEM)*, 2026, pp. 1–8.

[17] M. S. Mirazimi, C. Chen, P. Pescetto, S. Ferrari, G. Pellegrino, M. Diana, and T. Thiringer, "Accurate modeling of variable- flux pmsms without electromagnetic co-simulation," in *2024 International Symposium on Power Electronics, Electrical Drives, Automation and Motion (SPEEDAM)*, 2024, pp. 625–630.

[18] C. Chen, P. Pescetto, S. Ferrari, G. F. Olson, M. Diana, T. Thiringer, and G. Pellegrino, "Fast determination of feasible torque-speed range for variable flux machines including remagnetization voltage limit," in *2025 IEEE Energy Conversion Conference Congress and Exposition (ECCE)*, 2025, pp. 1–8.

[19] H. Cai and D. Hu, "On pmsm model fidelity and its implementation in simulation," in *2018 IEEE Energy Conversion Congress and Exposition (ECCE)*, 2018, pp. 1674–1681.

[20] C. Kukura, J. Apsley, and S. Djurovic, "Dynamic dq model of pmsm using fe-based luts," *IET Electric Power Applications*, vol. 19, no. 1, p. e70037, 2025.

[21] R. Garino, P. Pescetto, C. Chen, S. Ferrari, M. Diana, and G. Pellegrino, "Accurate simulation model of variable flux machines under asymmetrical demagnetization without fea co-simulation," in *2025 IEEE Energy Conversion Conference Congress and Exposition (ECCE)*, 2025, pp. 1–8.

[22] G. Pellegrino, R. I. Bojoi, and P. Guglielmi, "Unified direct-flux vector control for ac motor drives," *IEEE Transactions on Industry Applications*, vol. 47, no. 5, pp. 2093–2102, 2011.

[23] A. Athavale, K. Sasaki, T. Kato, and R. D. Lorenz, "Magnetization state estimation in variable-flux pmsms," in *2017 IEEE International Electric Machines and Drives Conference (IEMDC)*, 2017, pp. 1–8.

[24] S. Beck, J. Kesten, and M. Doppelbauer, "A review on flux estimation methods for variable flux machine applications," in *2025 Energy Conversion Congress Expo Europe (ECCE Europe)*, 2025, pp. 1–6.

[25] P. Jansen and R. Lorenz, "A physically insightful approach to the design and accuracy assessment of flux observers for field oriented induction machine drives," *IEEE Transactions on Industry Applications*, vol. 30, no. 1, pp. 101–110, 1994.

[26] A. Vagati, M. Pastorelli, G. Franceschini, and V. Drogoreanu, "Digital observer-based control of synchronous reluctance motors," in *IAS '97. Conference Record of the 1997 IEEE Industry Applications Conference Thirty-Second IAS Annual Meeting*, vol. 1, 1997, pp. 629–636 vol.1.

[27] L. Harnefors, "Design and analysis of general rotor-flux-oriented vector control systems," *IEEE Transactions on Industrial Electronics*, vol. 48, no. 2, pp. 383–390, 2001.